ACADEMIC PRESS

Available online at www.sciencedirect.com
SCIENCE DIRECT®

Journal of Catalysis 217 (2003) 172–185

JOURNAL OF CATALYSIS

www.elsevier.com/locate/jcat

Selective catalytic reduction of NO with NH_3 over mesoporous V_2O_5–TiO_2–SiO_2 catalysts

V.I. Pârvulescu,[a] S. Boghosian,[b] V. Pârvulescu,[c] S.M. Jung,[d] and P. Grange [d,*]

[a] *Department of Chemical Technology and Catalysis, Faculty of Chemistry, University of Bucharest, B-dul Republicii 13, Bucharest 70346, Romania*
[b] *Department of Chemical Engineering, University of Patras and Institute of Chemical Engineering and High Temperature Chemical Processes (FORT/ICE-HT), PO Box 1414, GR-26500, Patras, Greece*
[c] *Institute of Physical Chemistry of the Romanian Academy of Sciences, Splaiul Independentei 202, Bucharest, Romania*
[d] *Unité de catalyse et chimie des matériaux divisés, Université catholique de Louvain, Croix du Sud 2/17, 1348 Louvain-la-Neuve, Belgium*

Received 15 October 2002; revised 6 January 2003; accepted 6 January 2003

Abstract

Mixed vanadia–titania–silica catalysts (3 or 6 wt% V_2O_5, and 16–34 wt% TiO_2) were one-pot prepared by sol–gel and hydrothermal methods in the presence of surfactants. Sodium silicate (25.5–28.5% silica) or tetraethylorthosilicate was used as a precursor for silica; tetraisopropylorthotitanate or titanyl acetylacetonate, for titania; and vanadyl sulfate or vanadium acetylacetonate, for vanadia. Cetyltrimethylammonium bromide, octadecyltrimethylammonium bromide, or dodecylamine was used as a surfactant. The catalysts were characterized by adsorption and desorption curves of N_2 at 77 K, NH_3-DRIFTS, H_2-TPR, XRD, in situ Raman spectroscopy, XPS, and TEM. The catalysts were tested in NO reduction with ammonia using a total flow rate of 100 ml/min and a feed composition of nitric oxide 0.1 vol%, ammonia 0.1 vol%, oxygen 3 vol%, in helium. Vanadia was found to be entrapped in these catalysts as V(V) species in which the population of V=O monomeric bonds strongly depended on the dispersion. Titanium also existed in a very oxidated state, and for high dispersions it adopted a tetrahedral coordination. These structures led to surfaces on which mainly Lewis acid sites are effective under reaction conditions. Under such conditions, the dominant route followed an Eley–Rideal mechanism, yielding in such a way very high activity and selectivity. A comparison with a conventional V_2O_5–TiO_2 catalyst led to the conclusion that the intrinsic activity of one-pot prepared polymeric sol–gel catalysts is higher.

Keywords: Sol–gel prepared vanadia–titania–silica catalysts; NO reduction with NH_3; NH_3 diffuse reflectance infrared Fourier transform spectroscopy; H_2 temperature-programmed reduction; X-ray diffraction; In situ Raman spectroscopy; X-ray photoelectron spectroscopy; Transmission electron microscopy

1. Introduction

In selective catalytic reduction (SCR), V_2O_5 supported on TiO_2 represents the conventional composition and shows high activity [1]. However, in practical application, TiO_2 exhibits several drawbacks such as poor mechanical strength, low surface area, and high cost. To improve properties, many methods have been developed and applied [2–5]. Studies concerning the modification of TiO_2 properties by addition of other metal oxides have attracted much interest [6–11]. Among these, articles have explained strong interaction between TiO_2 and SiO_2 [12–21].

Several studies reported the application of V_2O_5–TiO_2–SiO_2 catalysts in SCR using various preparation methods. Almost all these preparations considered the deposition of vanadium on mixed TiO_2–SiO_2 oxides prepared either by coprecipitation or by the sol–gel method. Shikada et al. [22] and Odenbrand et al. [23] prepared mixed TiO_2–SiO_2 oxides by coprecipitation and vanadium was subsequently introduced by impregnation with NH_4VO_3. Shikada et al. [22] and Vogt et al. [24] proposed a procedure in which both titanium and vanadium were introduced by impregnation from several precursors. Rajadhyaksha et al. [25] prepared silica-supported titania samples and then V_2O_5 was impregnated on these supports. They observed a higher intrinsic activity on V_2O_5–TiO_2–SiO_2 than on V_2O_5–SiO_2. Silica-supported vanadia catalysts require a higher vanadia content to reach a conversion similar to that of titania- or

* Corresponding author.
E-mail address: grange@cata.ucl.ac.be (P. Grange).

0021-9517/03/$ – see front matter
doi:10.1016/S0021-9517(03)00028-9

alumina-supported catalysts. In addition, they found that the TiO_2 content is significant in increasing SCR activity. Handy et al. [26] also prepared V_2O_5–TiO_2–SiO_2 catalysts by reacting vanadyl triisopropoxide with sol–gel-prepared TiO_2–SiO_2 mixed oxide. These authors indicated that this might be a way to provide highly active and stable catalysts, if the titania is partly present in crystalline form. Reiche et al. reinvestigated the structural properties of these catalysts [27] and showed that vanadia grafted on TiO_2–SiO_2 shows lower intrinsic activity than V_2O_5–TiO_2 prepared by the sol–gel method but no deactivation was observed on these catalysts. Studies reported recently by Sorrentino et al. [28] confirmed this behavior attributing the performance of vanadia grafted on TiO_2–SiO_2 catalysts to the size of the V_2O_5 clusters.

From previous results, it can be concluded that the degree of interaction between TiO_2 and V_2O_5 in V_2O_5–TiO_2–SiO_2 is a dominant factor in SCR activity and the preparation method is very important in determining the effective structure of V_2O_5–TiO_2–SiO_2. To find a way to obtain a high degree of interaction between TiO_2–V_2O_5 in V_2O_5–TiO_2–SiO_2 without loss of surface area and with improved physical properties, attempts at a new preparation of V_2O_5–TiO_2–SiO_2 are of interest.

The aim of this work is to prepare one-pot V_2O_5–TiO_2–SiO_2 catalysts using the sol–gel technique and to elucidate if the behavior of V_2O_5–TiO_2–SiO_2 with higher SCR activity is related to the increased selective interaction between V_2O_5–TiO_2 in TiO_2–SiO_2 support. The samples have been prepared by co-addition of the V_2O_5 precursor during the preparation of Ti-MCM41-like structures. A thorough characterization of these catalysts has been made to determine the influence of the preparation method on catalyst structure, then their catalytic behavior in SCR of NO with NH_3 was investigated and discussed.

2. Experimental

2.1. Catalyst preparation

Mixed vanadia–titania–silica catalysts were one-pot prepared by the sol–gel method in the presence of the surfactants. The sols obtained were gelatinized at room temperature (VTSN2–VTSN8) or hydrothermally treated after a gelation time (VTSN1, VTSN9).

The molar compositions of the synthesized $V_{2l}O_5/TiO_2/SiO_2$ gels were $1.00/0.28/0.022$, $1.00/0.14/0.022$, and $1.00/0.14/0.06$. The reagents used as precursors were sodium silicate (25.5–28.5% silica) (SS) or tetraethylorthosilicate (TEOS), for silica; tetraisopropylorthotitanate (TIPOT) or titanyl acetylacetonate (TA), for titania; and vanadyl sulfate (VS) or vanadyl acetylacetonate (VA), for vanadia. Cetyltrimethylammonium bromide (CTMABr), octadecyltrimethylammonium bromide (ODTMABr), and dodecylamine (DA) were used as surfactants. For comparison VTSN3 catalyst was prepared without surfactant. Commercial reagents were used as received.

VTSN1 sample was synthesized by hydrothermal treatment on the basis of molar gel composition of $1.00SiO_2$:$0.28TiO_2$:$0.045VO_x$:0.47CTMABr:$0.28Na_2O$:3.2TMAOH:$186H_2O$. Vanadyl sulfate (solution 2 wt% in 2-propanol) and TA were added dropwise to a mixture of sodium silicate, water, and surfactant. After 2 h stirring, the tetramethylammonium hydroxide (25 wt% TMAOH in water) was added. The pH value of the gel was adjusted to 11 with H_2SO_4. The gel obtained was kept under vigorous stirring at room temperature overnight. After that, it was autoclaved at 373 K for 3 days. The solid products were recovered by filtration and washed with bidistilled water.

VTSN2–VTSN7 catalysts were obtained by the polymeric sol–gel method with a molar $SiO_2/TiO_2/V_2O_5$ ratio of $1.00/0.14/0.022$. The molar ratio of surfactant/silica was $0.2/1$. For VTSN2–VTSN4 samples, the sol–gels of silica (A) and titania (B) were obtained in two different ways. For A, a mixture of TEOS, ethanol, and water ($SiO_2/EtOH/H_2O$ for a molar ratio of $1/5.2/5.2$) was refluxed (pH 1) at 353 K for 2 h. Then, the sol–gel obtained was cooled to room temperature. For B, a mixture of TIPOT, 2-propanol, and acetic acid ($TIPOT/C_3H_7OH/CH_3COOH$ molar ratio $1/9.5/1.5.2$) was stirred for 3 h. CTMABr solution (C) was obtained by mixing CTMABr with water for 1 h. Vanadyl sulfate was added, under stirring, to mixture B. Solution C was added either concomitantly in an A + B + C mixture (samples VTSN2 and VTSN4) or to the premixed A + B mixture (sample VTSN3) and the gelation was carried out at room temperature. For VTSN4, acetylacetone was added to B after the addition of vanadyl sulfate (the amount of acetylacetone was calculated as function of TiO_2; the molar TiO_2/acetylacetone ratio was $1/0.15$).

VTSN5–VTSN7 samples were prepared by first mixing the silica sol–gel (A) with the titania sol (B). For these catalysts, the mixture (B) was obtained by mixing a solution of TIPOT in 2-propanol with acetylacetone and vanadyl sulfate. Solution C was added to the A + B mixture and the gelation was carried out at room temperature. The composition of the gel was $1.00SiO_2$:$0.14TiO_2$:$0.022V_2O_5$ for VTSN6 and VTSN7, and $1.00SiO_2$:$0.14TiO_2$:$0.06V_2O_5$ for VTSN5. In the case of VTSN7 the surfactant was ODTMABr.

VTSN8 sample was prepared using TEOS, TIPOT, and vanadyl acetylacetonate as precursors and DA as surfactant. The $SiO_2/TiO_2/V_2O_5$ molar ratio was $1/0.14/0.022$. An alcoholic solution of TEOS, TIPOT, and vanadyl acetylacetonate in ethanol and 2-propanol (ethanol/SiO_2 molar ratio of 7, and 2-propanol/SiO_2 molar ratio of 1.5) was mixed with the solution of DA in water (DA/SiO_2 molar ratio of 0.3 and H_2O/SiO_2 molar ratio of 37). The mixture was homogenized under vigorous stirring at room temperature for 2 h, and then was aged for 12 h. The solid was filtered and washed.

VTSN9 was synthesized by hydrothermal treatment. The gel composition was: $1.00SiO_2$:$0.14TiO_2$:$0.045VO_x$:0.2 CTMABr:5.2ETOH; 1.0iPrOH:$0.07H_2SO_4$:$100H_2O$. The sol of silica with composition $1.0SiO_2/5.2EtOH/5.2H_2O$ and pH 1 was refluxed 2 h at 353 K and then cooled to room temperature (mixture A). Mixture B was obtained by mixing vanadyl sulfate, 2-propanol, and TA. CTMABr was dissolved in water slightly acidified with H_2SO_4 (mixture C). The three solutions were mixed and then added dropwise in water. The mixture was autoclaved at 373 K for 3 days.

All catalysts were dried at 373 K and calcined at 773 K, first in a nitrogen flow with a ramp of 2 K min^{-1} and then in an air flow for 6 h.

For comparison, a conventional V_2O_5–TiO_2 catalyst with 2.3 wt% V_2O_5 was prepared using a procedure described in a previous article [29].

2.2. Catalyst characterization

Elemental analysis of V, Ti, S, and Si was performed by atomic emission spectroscopy with inductively coupled plasma atomization (ICP-AES) after drying of the samples overnight at 373 K (Table 1). The sulfur content of the activated catalysts was less than 0.2 wt%. Adsorption and desorption curves of N_2 at 77 K were obtained with a Micromeritics ASAP 2000 apparatus after degassing the samples at 423 K for 12 h under vacuum.

2.2.1. DRIFTS

In situ diffuse reflectance infrared Fourier transform spectroscopy (DRIFTS) spectra were collected in a Bruker IFS88 infrared spectrometer with KBr optics and a DTGS detector. Pure samples were placed inside a commercial controlled environmental chamber (Spectra-Tech 0030-103) attached to a diffuse reflectance accessory (Spectra-Tech collector). To investigate the stability of the adsorbed ammonia species during temperature elevation, the spectra were recorded under helium (30 ml min^{-1}) at room temperature and 373, 523, and 573 K, after exposure to an ammonia flow for 30 min at room temperature.

2.2.2. Temperature-programmed reduction

Temperature-programmed reduction (TPR) measurements with H_2 were carried out in the same fixed bed quartz microreactor as that used for the catalytic testing. Four hundred milligrams of sample was heated from room temperature to 773 K at the rate of 1 K min^{-1} in a diluted flow of H_2 (5% H_2 in He at 27 ml min^{-1}) and kept at 773 K for 8 h. After being cooled to room temperature under H_2 flow, the sample was purged with He (15 ml min^{-1}) for 3 h. The H_2 and H_2O desorbed were analyzed with a Balzers Quadrupole QMG 311 mass spectrometer. Released amounts were determined from calibration of the MS signals and calculation of the peak areas using a subroutine program.

2.2.3. X-ray diffraction

The X-ray diffraction (XRD) patterns were recorded at 40 kV and 50 mA with a Siemens D-5000 diffractometer equipped with a variable-slit diffracted-beam monochromator and scintillation counter. The diffractograms were recorded in the range 0–80° 2θ min^{-1} using Cu-K_α radiation ($\lambda = 1.54183$ Å).

2.2.4. Transmission electron microscopy

TEM analysis was done with a Tecnai Philips microscope with an accelerating voltage of 100 kV.

2.2.5. In situ Raman spectra

In situ Raman spectra were obtained using $\sim$ 150-mg samples of the catalysts, which were pressed into self-supporting wafers and mounted on an adjustable holder in the center of the in situ Raman furnace, which is mounted on a xyz plate. Temperature was controlled with a thermocouple placed inside the holder, near the catalyst. The gases used were O_2 (L'Air Liquide 99.995% purity), 10,000 ppm NH_3/N_2 and NO/N_2 mixtures (L'Air Liquide), and N_2 (L'Air Liquide 99.999%) as a balance gas and were mixed using electronic mass flowmeters (Brooks Instruments Model 5850E). The gas feed consisted of 2000 ppm NO, 2200 ppm NH_3 (ratio $NH_3/NO = 1.1$), and 2% O_2 balanced in N_2 or various mixtures of these at a total feed flow rate of 50 cm^3 min^{-1}.

In situ Raman spectra were excited using the 488.0-nm line of an Ar^+ ion laser (Spectra Physics Model 164), which

Table 1
Chemical composition of the investigated catalysts

Catalyst	Surfactant	Vanadium precursor	Titania precursor	Silica precursor	Chemical composition (wt%)		
					SiO_2	TiO_2	V_2O_5
VTSN1	CTMAB2	VS	TA	SS	71	26	3
VTSN2	CTMAB2	VS	TIPOT	TEOS	81	16	3
VTSN3	CTMAB2	VS	TIPOT	TEOS	81	16	3
VTSN4	CTMAB2	VS	TIPOT	TEOS	81	16	3
VTSN5	CTMAB2	VS	TIPOT	TEOS	62	32	6
VTSN6	CTMAB2	VS	TIPOT	TEOS	63	34	3
VTSN7	ODTMAB2	VS	TIPOT	TEOS	62	32	6
VTSN8	DA	VA	TIPOT	TEOS	81	16	3
VTSN9	CTMAB2	VS	TA		71	26	3

was focused on the catalytic wafer by a cylindrical lens and operated at a power level of 30 mW at the sample. The scattered light was collected at 90° (horizontal scattering plane), analyzed with a 0.85-m Spex 1403 double monochromator, and detected by a −20 °C cooled RCA photomultiplier equipped with EG&G photon counting electronics.

Each sample was oxidized for 1 h in the in situ Raman furnace at 400 °C in pure flowing O_2. Raman spectra were then recorded successively in O_2, NH_3/N_2, $NH_3/NO/N_2$, $NH_3/NO/O_2/N_2$, and O_2 at 400 °C, after at least 1 h of gas treatment. At the end of each sequence the sample was reoxidized and a spectrum was taken to confirm that the catalyst was reestablished in its initial oxidized state.

2.2.6. X-ray photoelectron spectroscopy

The X-ray photoelectron spectra were recorded using an SSI X probe Fisons spectrometer (SSX-100/206) with monochromated Al-K_α radiation. The spectrometer energy scale was calibrated using the Au $4f_{7/2}$ peak (binding energy 84.0 eV). The samples were moderately heated with a quartz lamp in the introduction chamber of the spectrometer to promote degassing, thus improving the vacuum in the analysis chamber. For the calculation of binding energies, the C 1*s* peak of the C–(C,H) component at 284.8 eV was used as an internal standard. The values collected for Si $2p$ constituted an additional indication of the validity of binding energies. The composite peaks were decomposed by a fitting routine included in the ESCA 8,3 D software. The superficial composition of the investigated samples was determined using the same software. The bands assigned to V, Ti, S, and Si $2p$ were considered.

2.3. Catalytic activity

Activity measurements were performed in a continuous-flow fixed bed reactor operating at atmospheric pressure. A 0.08-g sample was used in this work. The total flow rate was 100 ml min^{-1} and the feed composition was nitric oxide 0.1 vol%, ammonia 0.1 vol%, oxygen 3 vol%, in helium. The inlet and outlet gas compositions were measured using a quadrupole mass spectrometer QMC 311 Balzers coupled to the reactor.

3. Results

3.1. Textural characteristics

Table 2 gives the textural characteristics of the investigated catalysts. Mean pore size was determined from BJH formalism considering the hysteresis desorbtion branch. Only VTSN4–VTSN8 exhibited monomodal pore size distribution. For VTSN4–VTSN8 both the shape of the adsorption–desorption isotherms of N_2 at 77 K and the pore size distribution suggest that these correspond to typical mesoporous materials. However, the comparison of *t*-plot and BET surface areas indicated that a certain percentage of micropores (to a lesser extent for VTSN1 and VTSN4–VTSN8) exist in all the catalysts investigated. Of course for VTSN3 and VTSN9 the presence of micropores is almost excluded because the surface areas are too small.

Table 2
Textural characteristics of the catalysts

Catalyst	BET surface area ($m^2\ g^{-1}$)	BJH desorption average pore diameter (nm)	Pore volume ($cm^3\ g^{-1}$)
VTSN1	35	48.1	0.32
VTSN2	239	7.3	0.16
VTSN3	14	30.3	0.07
VTSN4	709	5.5	1.17
VTSN5	1206	3.7	0.53
VTSN6	994	2.1	0.52
VTSN7	873	3.3	0.43
VTSN8	649	5.5	0.72
VTSN9	8	67.7	0.02

Table 2 provides evidence of the effect of the preparation procedures. It is worth noting that these preparations were repeated and the textural characteristics were measured again to confirm the effect of the preparation parameters. A high surface area and a monomodal pore size distribution mean a well-disposed architecture and this seems to be the contribution of the advanced homogeneity of the three components, namely, vanadium, titanium, and silicon. Several factors seem to provide support for such a homogeneity: (i) the presence of the surfactant (see VTSN2 vs VTSN3) and its length (see VTSN5 vs VTSN7); (ii) the way in which the sol–gel method is carried out (VTSN2 vs VTSN5), and the presence of hydrolysis controllers like acetylacetone (see VTSN2 vs VTSN4); (iii) the nature of the precursors (see VTSN1 and VTSN9). The use of titanium acetylacetonate in these syntheses seems to be detrimental to achieving good textural properties.

Textural measurements determined for the samples subjected to the catalytic tests for 6 h showed no change in surface area or pore size distribution.

3.2. XRD

Except for VTSN1 and VTSN9 no lines due to species other than silica or to a mesoporous texture were observed. The patterns of VTSN1 and VTSN9 show a very weak shoulder at 2θ 25.64 which is very difficult to assign. It may correspond either to a cluster of a vanadium oxide, V_6O_{13} [30], or to anatase crystalline titania particles [20]. The peaks in the region 2θ smaller than 5 suggest a mesoporous-like organization. The broadband centered at 2θ 20–25 is assigned to silica.

3.3. H_2-TPR

Fig. 1 gives the H_2-TPR profiles of several catalysts in comparison with a conventional V_2O_5/TiO_2 catalyst. High-surface-area mixed oxides exhibit peaks with a small

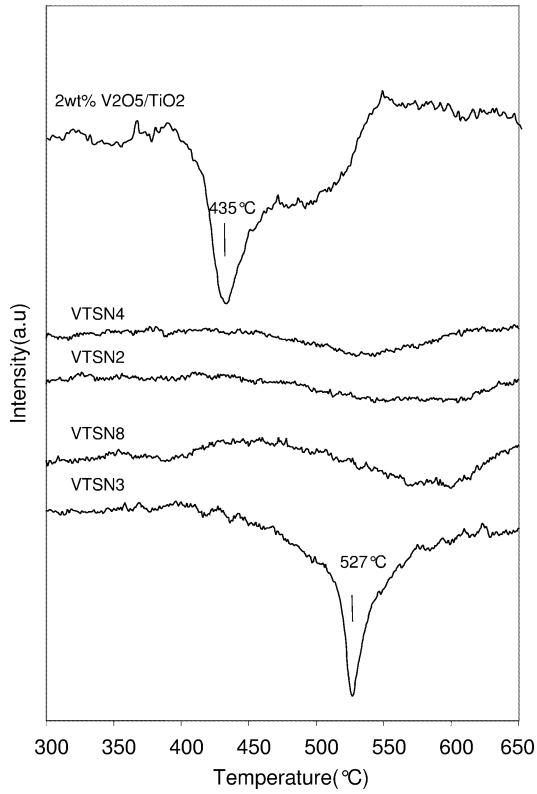

Fig. 1. H_2-TPR profiles of VTSN samples compared with the conventional V_2O_5–TiO_2 catalyst.

area located at high temperatures. VTSN3, which has a small surface area (see Table 2), exhibits a high hydrogen consumption associated with a peak located at 800 K. Such behavior may suggest that vanadia is agglomerated in this catalyst at least to a certain level. Large peaks were also determined for the commercial V_2O_5/TiO_2 catalyst but these were located at much lower temperatures, namely, 708 and 783 K.

3.4. XPS

Table 3 compiles the XPS data measured for the investigated catalysts. Except for VTSN1 and VTSN9, binding energies for V $2p_{3/2}$ species indicated the existence of vanadium in a (V) oxidation state. Berry et al. [31] reported for V $2p_{3/2}$ in a V(V) oxidation state a binding energy of 517.7 eV, which is very close to the values measured for samples VTSN2–VTSN8. VTSN5 exhibited the highest binding energy. The smaller values determined for VTSN1 and VTSN9 may correspond to a partial reduction to V(IV) [32]. The same behavior was also determined for binding energies of Ti $2p_{3/2}$ species. Except for the VTSN1 and VTSN9 samples, the binding energies were very close to those of Ti(IV) [33]. These two samples might contain a part of Ti(III). In addition, these data may give some information about the coordination of titanium ions. According to several authors [27,34] a binding energy of 459.5 eV is typical of tetrahedrally coordinated titanium, while energies of about 458.5 eV indicate the presence of some octahedrally coordinated titanium in the sample.

O 1*s* binding energies associated with oxygen in Ti–O and Si–O bonds varied in a limited range. A tendency toward more oxidized species was again found for VTSN5.

The relative XPS atomic ratios may give in this case useful information about the dispersion. Table 3 compares XPS and chemical ratios. The V/(Ti + Si + V) ratios were almost the same, even if very small differences were found for VTSN4 and VTSN7. Nevertheless, these two samples contain twice the vanadium of the other samples and the calculated XPS ratios might be evidence of very good dispersions. Very good dispersions were also found for titanium. A very weak tendency for superficial agglomeration might be supposed only for VTSN9.

3.5. In situ Raman spectra

For brevity, the discussion in this section concerns the catalysts that exhibit either very high or very low SCR catalytic activity, namely, VTSN5 and VTSN1. These samples constitute, as will be demonstrated in the relevant section, the two "extreme" cases in reactivity. A correlation between the structural and vibrational properties of the dispersed surface vanadia species and the textural and catalytic properties of these samples is attempted.

Fig. 2 illustrates sequential in situ Raman spectra of the VTSN5 catalyst recorded after exposure to the various

Table 3
XPS binding energies, relative XPS ratios, and chemical ratios

Catalyst	Binding energy (eV)					Relative XPS ratios		Chemical ratios	
	Ti $2p_{3/2}$	Si $2p$	V $2p_{3/2}$	Ti–O 1*s*	Si–O 1*s*	V/(Ti+Si+V)	Ti/(Ti+Si+V)	V/(Ti+Si+V)	Ti/(Ti+Si+V)
VTSN1	458.8	103.3	516.8	530.4	532.5	0.17	0.06	0.023	0.21
VTSN2	459.4	103.6	517.4	530.7	532.8	0.17	0.08	0.023	0.13
VTSN3	459.5	103.3	517.5	531.2	532.6	0.17	0.09	0.023	0.13
VTSN4	459.4	103.8	517.4	530.8	533.0	0.20	0.08	0.023	0.13
VTSN5	459.5	103.8	517.8	531.0	533.1	0.26	0.07	0.047	0.28
VTSN6	459.3	103.6	517.4	530.7	532.9	0.17	0.08	0.023	0.28
VTSN7	459.3	103.6	517.5	530.7	532.9	0.28	0.08	0.047	0.28
VTSN8	459.5	103.7	517.4	531.0	532.9	0.16	0.06	0.023	0.13
VTSN9	458.5	103.1	516.9	530.5	532.4	0.21	0.10	0.023	0.21

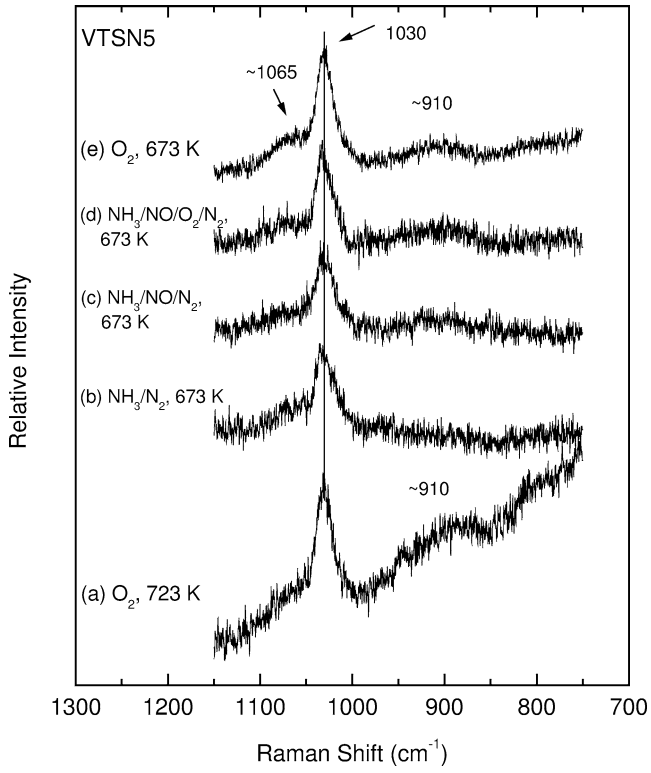

Fig. 2. Sequential in situ Raman spectra of VTSN5 catalyst: (a) at 723 K under pure O_2 right after calcination in the Raman furnace; (b) at 673 K under NH_3/N_2; (c) at 673 K under $NH_3/NO/N_2$; (b) at 673 K under $NH_3/NO/O_2/N_2$; (e) at 673 K after reoxidation with pure O_2. Laser wavelength; $\lambda_0 = 488.0$ nm; laser power, $I_0 = 60$ mW; scan rate, sr $= 6$ cm^{-1} min^{-1}; time constant, $\tau = 1$ s; spectral slit width, ssw $= 8$ cm^{-1}.

$NH_3/NO/O_2/N_2$ gas atmospheres indicated in the figure. Spectrum 2a is taken under O_2 at 723 K right after the catalyst calcination (at 773 K) in the Raman furnace. This spectrum represents the fully oxidized state of the catalyst under dehydration conditions and shows that dispersed vanadia is present predominantly in the form of mono-oxo monomeric vanadyl species with the characteristic V=O stretch at 1030 cm^{-1} possessing probably a distorted tetrahedral configuration with three anchoring V–O–M bonds. The literature abounds with assignments of sharp bands in the region 1026–1042 cm^{-1} to V=O modes of isolated O=V–(O–M)$_3$ species, observed under dehydration conditions for V_2O_5 catalysts supported on various oxides [35–47]. Furthermore, a broad feature centered at ~ 910 cm^{-1} indicates the possible presence of polymeric vanadates [35–44]. This is in agreement with recently reported Raman spectra of a VO_x-MCM catalyst, in which a sharp band at 1040 and a broadband at ~ 920 cm^{-1} were assigned to V=O modes of monomeric surface VO_4 species and to stretching vibrations of terminal vanadyl groups within a two-dimensional surface phase, respectively [47]. However, the assignment of this band requires caution since it has been demonstrated that such a weak and broadband at ~ 915 cm^{-1} for V_2O_5/SiO_2 and $V_2O_5/TiO_2/SiO_2$ catalyst samples most likely originates from silica (Si–O) functionalities, indicative of formation of V–O–Si bonds [45,48]. Significantly, a band at 1060–1070 cm^{-1}, assigned also to the same silica functionalities, appears together with the ~ 915 cm^{-1} band [45,48] and this is also the case in Fig. 2 (spectra a and e). Furthermore, no crystalline vanadia is present, judged by the absence of its characteristic 994 cm^{-1} band. Therefore, it is more likely that vanadia occurs exclusively in the form of isolated O=V–(O–M)$_3$ species at the dehydrated catalyst surface. Thus, a very good dispersion of vanadia must prevail in the case of VTSN5. However, Raman experiments alone cannot allow us to deduce whether an isolated VO_4 unit possesses only three oxygenated Si(IV)–O$^-$ ligands or only three Ti(IV)–O$^-$ ligands or a combination of the two types [48]. Finally, it should be pointed out that the strong background seen in spectrum 2a does not reappear after cycling the catalyst under $NH_3/NO/O_2/N_2$ conditions.

Spectrum 2b is obtained at 673 K after 4 h of exposure to NH_3/N_2 flow and the following observations can be made. (A) The 1030 cm^{-1} V=O band has lost some of its intensity and appears to have a low-frequency shoulder indicating that adsorption/coordination of NH_3 perturbs the V=O groups of the monomeric species and elongates certain V=O bond distances. (B) The broad feature at ~ 910 cm^{-1} is no longer observed. Thus, if the band was due to polymeric vanadates, it appears that the polymers have been reduced. But, as mentioned above, the ~ 910 cm^{-1} band originates most probably from Si–O functionalities of V–O–Si bonds [45,48] and its disappearance would imply severe perturbation of a number of such bonds on exposure to NH_3.

Spectrum 2c is obtained at 773 K under flowing $NH_3/NO/N_2$ (after 1 h of exposure) and it is evident that admission of NO along with NH_3/N_2 does not induce significant changes compared with spectrum 2b except for a partial reappearance of the ~ 910 cm^{-1} band, indicating that the state of the surface species is not affected much by the presence of NO. After 1 h of exposure to reaction mixture $NH_3/NO/O_2/N_2$ (spectrum 2d) the intensities of the ~ 910 and 1030 cm^{-1} bands are almost restored and the spectrum resembles that of the fully oxidized catalyst. However, the overall shape of the 1030 cm^{-1} band remains asymmetric, still possessing a low-frequency shoulder, indicating that during reaction there is still (although to a less extent) perturbation of the V=O bonds which was found to be caused by the presence of NH_3. Finally spectrum 2e shows that after reoxidation at 673 K, the spectral features of the fully oxidized catalyst are restored and the 1030 cm^{-1} band regains its former intensity and symmetric shape. Close inspection of Fig. 2 reveals that the restoration of spectral features of the fully oxidized catalyst began when NO was added into the NH_3/N_2 feed (see Fig. 2c, partial reappearance of the ~ 910 cm^{-1} band). This is explained by taking into account that adsorbed NH_3 reacts with NO and thus its surface concentration is diminished in the presence of NO in the catalyst environment. On the other hand, it is well known that O_2 accelerates the SCR of NO by NH_3. So, the concentration of adsorbed NH_3 is expected to be

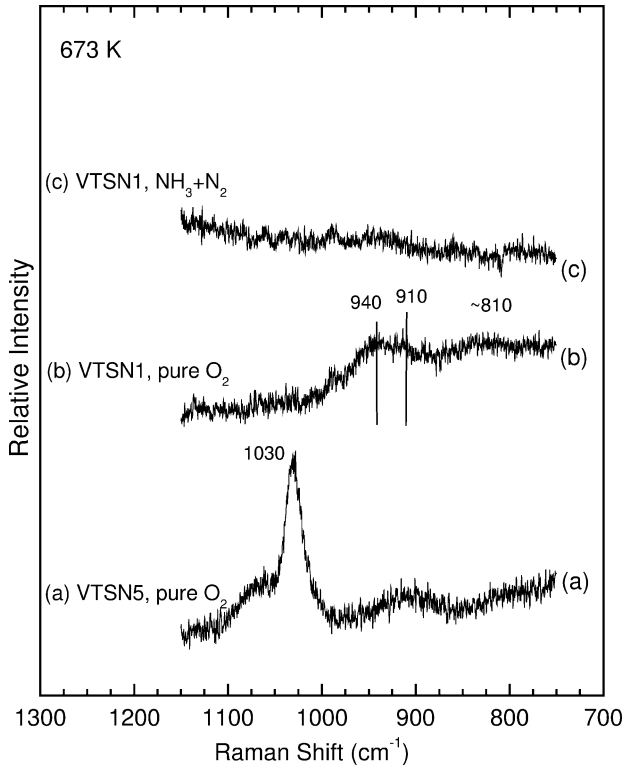

Fig. 3. In situ Raman spectra obtained at 673 K for: (a) VTSN5 under pure O_2; (b) VTSN1 under pure O_2; and (c) VTSN1 under NH_3/N_2. $\lambda_0 = 488.0$ nm; $I_0 = 60$ mW; sr $= 6$ cm^{-1} min^{-1}; $\tau = 1$ s; ssw $= 8$ cm^{-1}.

further diminished, and in turn the spectral features of the fully oxidized catalyst to be approached, on O_2 addition in the gas feed.

Figure 3 compares the in situ Raman spectra of VTSN5 and VTSN1 at 673 K under pure flowing O_2 (spectra 3a and 3b) and shows also the VTSN1 catalyst under NH_3/N_2 (after 1 h of exposure). Spectrum 3b shows that VTSN1, in its fully oxidized state, does *not* contain isolated monovanadate (VO_4) species, as can be seen from the absence of the characteristic band in the 1030 cm^{-1} region. Furthermore, no band indicative of crystalline V_2O_5 formation is found in the characteristic 994 cm^{-1} position. The observed bands include a broad feature centered at ~ 925 cm^{-1} with components at 940 and 910 cm^{-1} and another broadband centered at ~ 810 cm^{-1}. The assignment of the band in the vicinity of 910 cm^{-1} requires caution since, apart from polymeric vanadates, Si–O functionalities also give rise to bands in the same region, as mentioned above [45,48]. However, the absence of the 1065 cm^{-1} silica band, which should also be observed if the 910 cm^{-1} shoulder was due to silica, allows us to safely assume that there is no contribution of Si–O functionalities to the 910–940 cm^{-1} feature. Thus, the VTSN1 catalyst in its fully oxidized state contains vanadia exclusively in the form of polymeric vanadates, probably in the form of corner-sharing VO_4 tetrahedra with one or two V–O–V bonds per vanadium [49,50]. The bands in the region 910–940 cm^{-1} can be assigned to terminal V=O modes of polymeric vanadates as proposed earlier [35,42,43] and the broad 800–820 cm^{-1} feature may originate from V–O–V bridging modes [35,49]. The following considerations provide further support to this tentative assignment.

The bond lengths and bond orders of terminal V=O and bridging V–O–V bonds in mono- and polyvanadate species can be estimated from the following empirical formulas derived from examination of a large number of model compounds [51]:

$$\nu = 21349 \exp(-1.9176R), \tag{1}$$

$$\mathrm{BO} = \left[0.2912 \ln(21349/\nu)\right]^{-5.1}. \tag{2}$$

Here ν is the vibrational wavenumber (cm^{-1}), BO is the bond order, and R is the V–O bond length (angstroms). Eqs. (1) and (2) can be used alongside observed Raman wavenumbers (Figs. 2, 3) to check the consistency of proposed coordinations/assignments with the constraint that the sum of the bond orders of V–O bonds involving a particular V(V) atom should be 5 valence units (vu).

Thus for the 1030 cm^{-1} band seen for VTSN5 (Figs. 2a,e) which was assigned to V=O groups of isolated O=V–$(O–M)_3$ distorted tetrahedral species, Eqs. (1) and (2) lead to values of 1.88 for bond order and 1.58 Å for bond length. Therefore the remaining three V–O bonds (along V–O–M bridges) share a total of 3.12 vu, corresponding to an average bond order of 1.04 vu and bond length of 1.77 Å per anchoring V–O, and this provides a good check on the above constraint.

Likewise, if the ~ 925 cm^{-1} band (the one with the 910 and 940 cm^{-1} components) observed for VTSN1 (Fig. 3b) is assigned to V=O vibrations of polyvanadates, we obtain an average value of 1.58 vu for bond order and 1.64 Å for bond length. The bond order and bond length of the ~ 810 cm^{-1} band, which was tentatively assigned to V–O–V, are found to be 1.28 vu and 1.71 Å. Thus, these average bond order values allow for the suggested [50] molecular structure of a terminal V=O bond (1.58 bond order) with *two* bridging V–O–V (1.28 bond order and a total of $2 \times 1.28 = 2.56$) and *one* V–O–M bond (bond order close to unity) for the polymerized vanadate species. The broadness of the 925 and 810 cm^{-1} bands of course allows for alternative attributions of wavenumber values within the regions of the two broadbands to V=O and V–O–V modes, respectively. Eqs. (1) and (2) then lead o variations in the involved bond orders and lengths and can also lead to an alternative coordination around a portion of vanadium atoms in the polymerized vanadate, namely, the one with a terminal V=O bond, *one* bridging V–O–V, and *two* V–O–M bonds [49].

Exposure of the VTSN1 catalyst to NH_3/N_2 leads to near-to complete reduction of the polymeric vanadia species, as evidenced from the disappearance of the bands due to polymerized species in Fig. 3c. Unfortunately, the reduced surface vanadia species do not give rise to new Raman bands owing to their very weak or inactive Raman signal, most likely also because of the absence of the V=O functionality,

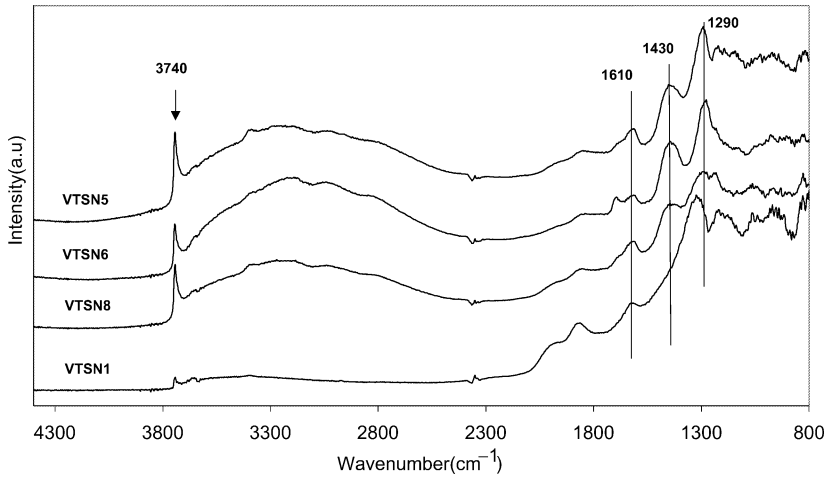

Fig. 4. NH_3-DRIFT spectra collected at 298 K for VTSN1, VTSN5, VTSN6, and VTSN8.

which is associated with a strong Raman signal [52]. The poor catalytic performance of VTSN1 might be explained by incorporation of vanadia in multilayers, thus making it inaccessible.

3.6. NH_3-DRIFT

Figs. 4–6 show the NH_3-DRIFT spectra collected at room temperature and at 373 and 523 K, respectively, for VTSN1, VTSN4, and VTSN5. Similar spectra were collected for the other catalysts investigated. These spectra contain bands due to ammonia adsorbed on both Brønsted (1430 cm^{-1}) and Lewis (1610 cm^{-1}) acid sites. The bands at 3372, 3274, 2994, 2790, and 1658 cm^{-1} after adsorption of NH_3 at room temperature are due to ν_{as}(N–H), ν_s(N–H), $2\delta_{as}$(H–N–H), $2\delta_s$(H–N–H), and δ_{as}(H–N–H) species adsorbed on Lewis acid sites of the surface [53]. The increase in temperature leads to a decrease in the intensity of the band located at 1430 cm^{-1}, which almost disappears at 523 K, indicating that under such conditions most of the ammonia is desorbed. A decrease in the intensity also occurs for the band due to ammonia adsorbed on Lewis acid sites, but these are still present after the temperature was raised to 523 K. The increase in temperature from 373 to 523 K leads to an increase in the V^{5+}=O overtone band intensity located at 1955 cm^{-1}. This corresponds to an advanced desorption of different N–H species.

3.7. TEM analysis

Figs. 7 and 8 are the TEM images corresponding to VTSN5 and VTSN1 catalysts which are the limit cases in terms of catalytic activity (see below). For VTSN5 an important part exists as typical MCM-41 organized material, as shown in Fig. 7. VTSN6 also shows this texture to a large extent, while for VTSN7 and VTSN4 this was evidenced to a smaller extent. An amorphous part is also present. For VTSN1 and VTSN9 only an amorphous phase was detected, while for the other samples the amorphous part was also dominant.

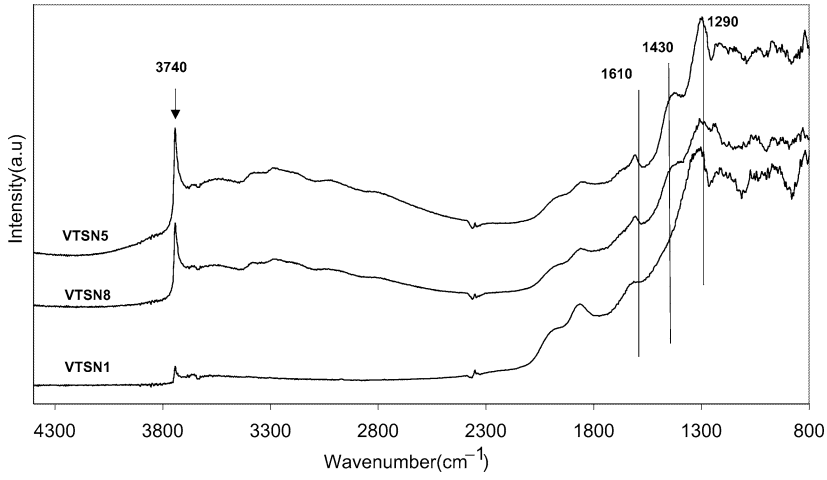

Fig. 5. NH_3-DRIFT spectra collected at 373 K for VTSN1, VTSN5, and VTSN8.

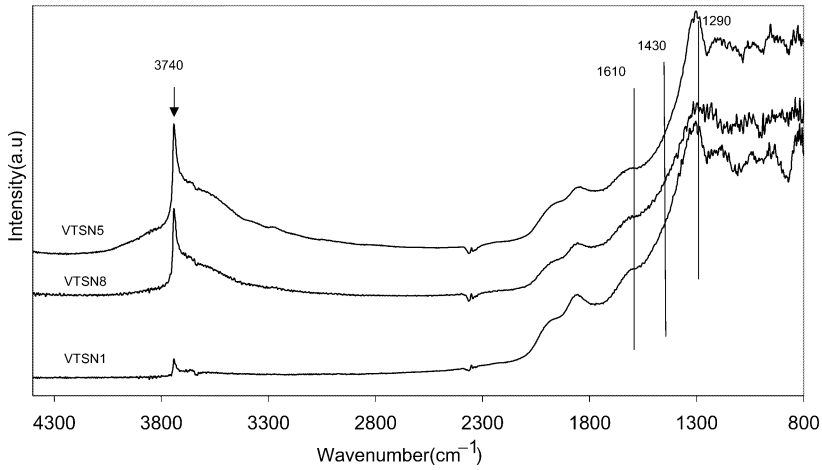

Fig. 6. NH_3-DRIFT spectra collected at 523 K for VTSN1, VTSN5, and VTSN8.

3.8. Catalytic data

Figs. 9 and 10 illustrate the catalytic performance of the catalysts in comparison with the commercial V_2O_5/TiO_2 catalyst. These data divide the mixed vanadia–titania–silica catalysts into three categories. The first corresponds to catalysts that exhibit no activity, namely, VTSN1 and VTSN9. Very surprisingly, these catalysts exhibit ammonia oxidation activity. On both catalysts, under the conditions of the investigation, about 15% of ammonia was oxidized to nitrogen and nitrogen oxide.

The second category concerns catalysts that show a conversion between 20 and 60%. A peculiarity of these catalysts is that the conversion increases monotonously with temperature up to 723 K. Typical SCR catalysts, as the V_2O_5/TiO_2 catalyst used for comparison in these experiments, exhibit a maximum of conversion in the range 573–623 K, followed at higher temperatures by a decrease in conversion.

The third category concerns the VTSN2, VTSN4, VTSN5, and VTSN7 catalysts. These catalysts show conversions in the range 40–90% but typical dependencies of the conversion on temperature, namely, a maximum in the range 573–623 K. The performance achieved with VTSN5 is noteworthy. The conventional V_2O_5/TiO_2 catalyst appears to be less active than VTSN4, VTSN5, and VTSN7.

Figs. 11 and 12 give the selectivity of these catalysts. The catalysts exhibit an almost total selectivity to nitrogen. It is worth noting that such an extremely high selectivity is preserved even at 623 K. Very high selectivity to nitrogen over the whole range of temperatures investigated was also achieved for VTSN3 and VTSN8. A very important aspect

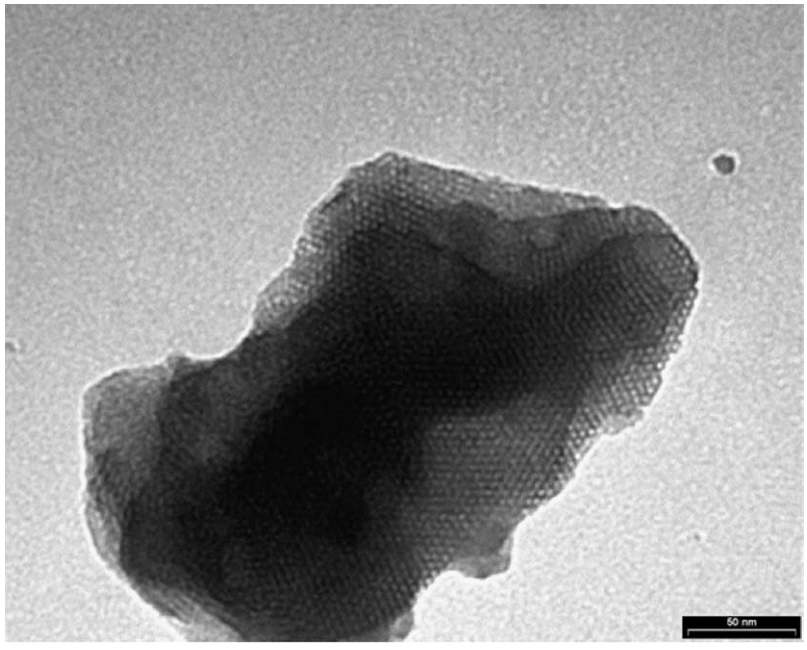

Fig. 7. TEM images corresponding to VTSN5.

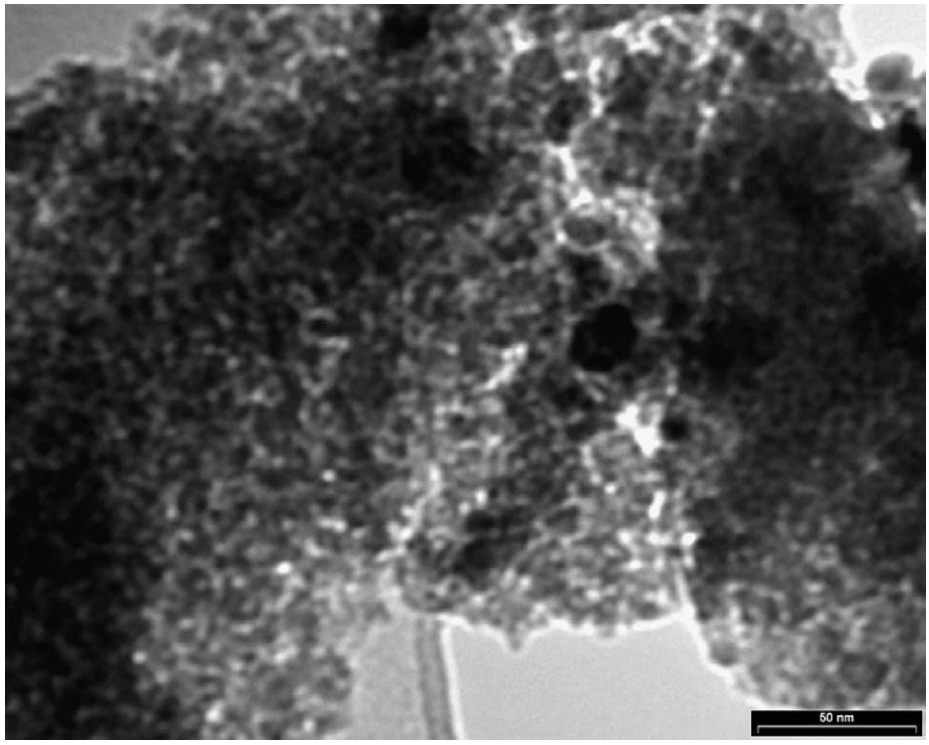

Fig. 8. TEM images corresponding to VTSN1.

related to the catalytic behavior of these catalysts is that, except for VTSN1 and VTSN9, which showed no activity in this reaction, all others showed higher selectivity than the conventional V_2O_5/TiO_2.

4. Discussion

4.1. Structural characteristics

One-pot preparation of mixed vanadia–titania–silica catalysts by the sol–gel method in the presence of the surfactants (VTSN2–VTSN8) or by hydrothermal treatments (VTSN1–VTSN9) led to different structures. The hydrothermal procedures led to amorphous materials with very small surface areas. A very small surface area was also obtained for VTSN3. For VTSN1 and VTSN9, vanadia was supposed to be partially segregated in clusters as shown by a very weak shoulder in XRD patterns. H_2-TPR profiles indicated a hydrogen consumption almost as large as that determined for a conventional V_2O_5/TiO_2 catalyst, which may also indicate the existence of the agglomerated species.

Contrarily to these samples, use of the sol–gel method in the presence of surfactants led to materials with very high surface areas (see Table 2). The structures resulting from these preparations were better organized, leading to

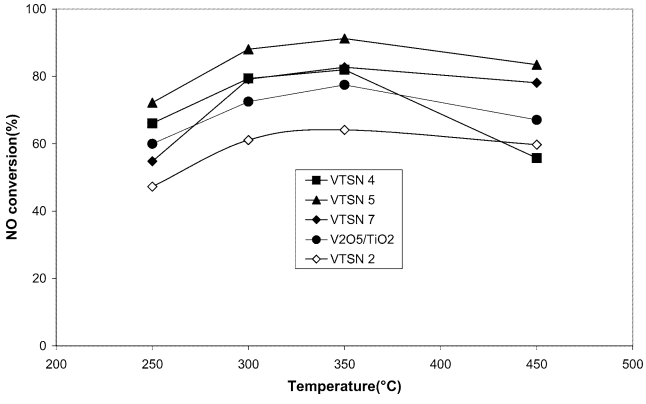

Fig. 9. Comparative catalytic performance of VTSN with the conventional V_2O_5/TiO_2 catalyst (0.08 g catalyst; flow rate 100 ml min^{-1}; feed composition: nitric oxide 0.1 vol%, ammonia 0.1 vol%, oxygen 3 vol%, in helium).

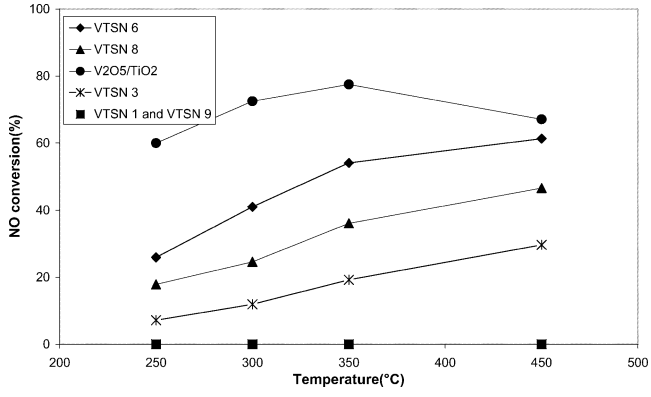

Fig. 10. Comparative catalytic performance of VTSN with the conventional V_2O_5/TiO_2 catalyst (0.08 g catalyst; flow rate 100 ml min^{-1}; feed composition: nitric oxide 0.1 vol%, ammonia 0.1 vol%, oxygen 3 vol%, in helium).

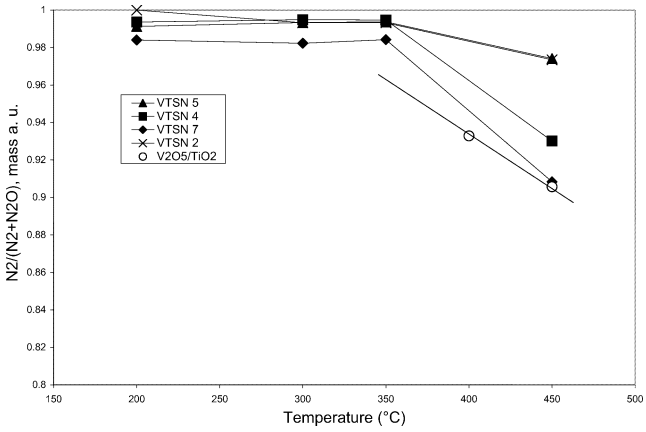

Fig. 11. Selectivity of VTSN catalysts compared with conventional V_2O_5/TiO_2 catalyst.

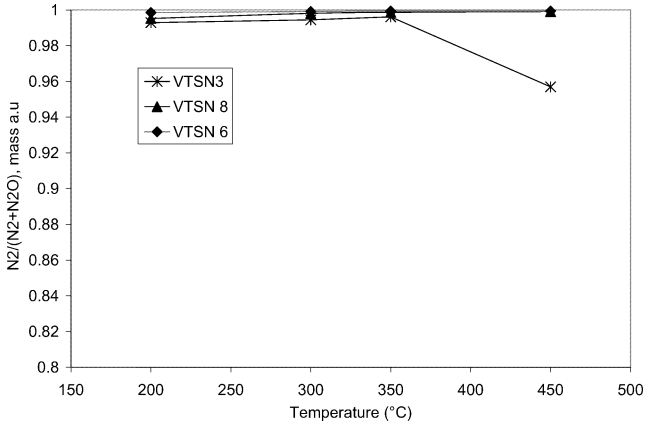

Fig. 12. Selectivity of VTSN3, VTSN6, and VTSN8 catalysts.

MCM-41-like textures as for VTSN5, VTSN6, and, into a smaller extent, VTSN7 and VTSN4. TEM analysis confirmed such behavior (Fig. 7). Monomodal pore size distribution was determined for these samples with a BJH diameter between 2 and 7 nm. These textures seemed to be fairly stable because no change was observed after 6 h reaction, neither from the adsorption–desorption curves of N_2 at 77 K nor from the TEM analysis. Vanadium is better dispersed in these structures, as seen both from the values of the XPS binding energies and from the Raman evidence of mono-oxo tetrahedral monomeric vanadyl species (shown, e.g., for VTSN5 in Figs. 2a and 2e). The same XPS investigation showed that titanium is tetrahedrally coordinated in these samples, while for VTSN1 and VTSN9 mainly the octahedrally coordinated titanium predominated. H_2-TPR profiles indicated a very small hydrogen consumption with peaks centered at high temperatures, namely, over 773 K. These results come in the same line with XPS data, indicating that for these catalysts both titanium and vanadium are more rigidified in defined surroundings, and with the Raman evidence for the dispersed vanadium oxide species (isolated VO_4 units), also indicative of defined surroundings. Naturally, based solely on Raman experiments it cannot be deduced whether an isolated VO_4 unit possesses only three oxygenated Ti(IV)–O^- ligands, or only three Si(IV)–O^- ligands, or a combination of the two types [48].

NH_3-DRIFT spectra indicated, for all the catalysts investigated, the existence of both Brønsted and Lewis acid sites. Spectra collected at high temperatures (523 K), namely, close to that of the catalytic conditions, indicated almost complete disappearance of the bands corresponding to Brønsted acidity, while those associated with Lewis acid sites were active. These investigations, using sensibly equal amounts of the sample, also showed that it is hard to distinguish between the different samples even if a slightly higher acidity was evidenced for VTSN5. The source of the acidity might be the linkage Ti–Si or V–Si or V–Ti. In the case of MCM-41 organized samples, and mainly for VTSN5, the acidity is expected to be improved because of the better dispersion of vanadium and titanium and because of the coordination adopted by these elements under such conditions.

4.2. Catalytic activity

The catalytic behavior was different for the various samples investigated: VTSN1 and VTSN9 exhibited no SCR activity, but were able to oxidize ammonia, VTSN3, VTSN6, and VTSN8 showed moderate activity, and the conversion increased monotonously with temperature up to 723 K, and VTSN4, VTSN7, and VTSN5 exhibited high SCR activity, the conversion per gram of catalyst being superior to that of V_2O_5–TiO_2.

From a textural point of view these categories correspond, first, to very low surface area materials, second, to nonregular mesoporous materials with monomodal pore size distribution and relatively high surface areas, and, third, to ordered materials containing an MCM-41-like phase. In VTSN5 the MCM-41 texture predominates. The surface area of these materials exceeds 700 $m^2\,g^{-1}$, reaching 1200 $m^2\,g^{-1}$ for VTSN5.

The catalytic behavior of the above catalysts is logically related to their structural properties. In the mechanism proposed by Topsøe and co-workers [54,55], it is suggested that both Eley–Rideal and Langmuir–Hinshelwood routes are possible but that NO more likely reacts as a weakly adsorbed species. They considered that vanadia–titania catalysts exhibit two separate catalytic functions, i.e., acid and redox functions. According to the above mechanism the catalytic cycle involves an acid site (V^{5+}–OH), the activation of adsorbed ammonia by the interaction with redox sites (V=O), the reaction of activated ammonia with gaseous or weakly adsorbed NO, and the recombination of surface hydroxyl groups.

XPS gave additional information about vanadia in these catalysts. Table 3 shows the smaller binding energies of V $2p_{3/2}$ species for samples VTSN1 and VTSN9, which exhibit practically no SCR catalytic activity. For the same samples, the binding energies of Ti $2p_{3/2}$ species correspond to an octahedrally coordinated state. Such a correlation

with the catalytic data indicates that better performance can be achieved with catalysts that contain vanadia in the (V) oxidation state and titanium as Ti(IV) in a typical tetrahedral coordination state. These structures correlate very well with a high dispersion of these species, deduced from the comparison of XPS and analytical data. VTSN5 exhibits the highest binding energies for vanadium and titanium in this series and also a better dispersion of these species.

Reducibility of these catalysts may also provide picture of their behavior in de-NO_x reactions. Roozeboom et al. [2] explained the decrease in reducibility of vanadia on the supports compared with TiO_2 by better contact with this support. Handy et al. [26] reported, for V_2O_5–TiO_2–SiO_2 catalysts containing crystalline TiO_2, higher reducibility as well as higher activity in the SCR of NO than for catalysts with amorphous TiO_2. Data obtained in this case show a different behavior. H_2-TPR profile determined for the V_2O_5–TiO_2 catalyst exhibits the same shape as that already reported by several groups [2,27]. VTSN catalysts with low activity also show H_2-TPR profiles similar to those reported for V_2O_5–TiO_2–SiO_2 obtained by grafting of vanadia on the sol–gel-prepared TiO_2–SiO_2 supports [27]. Both procedures may lead to clustered forms of vanadia. A completely different picture is obtained for the VTSN samples containing highly dispersed vanadia, for which hydrogen consumption was small and occurred at high temperatures. Actually these catalysts were those that showed higher catalytic performance in this reaction. These results raise questions about the direct correlation between the catalytic performance in SCR-deNO_x and the bulk reducibility of vanadia. On the basis of these data it appears that this condition is far from obligatory.

As a general mechanistic feature, ammonia is adsorbed over Lewis and/or Brønsted acid sites. This species is activated by means of dissociation of one hydrogen in ammonia through catalytic reduction, and then reaction with gas phase NO gives rise to a nitroamide intermediate, which decomposes to nitrogen and water [56–59]. The reduced catalyst sites are regenerated by oxidation with the oxygen in gas phase. However, when further increasing the reducibility around this species, the number of dissociable hydrogen atoms in one molecular ammonia progressively increases. This leads to an advanced oxidation of intermediate species by the oxygen belonging to the catalytic surface, finally inducing a higher rate of ammonia oxidation. On typical vanadium-based SCR catalysts, the temperature window of the SCR reaction, corresponding to high NO conversion and complete selectivity to nitrogen, is shifted toward lower temperature with increasing vanadia loading. It was suggested that this behavior is related to the presence of more labile oxygen atoms in high vanadium loadings. This is beneficial for activity but is also detrimental for the selectivity of the SCR reaction. Wachs et al. [60] suggested that SCR selectivity toward N_2 formation also varies with the immediate environment of the surface vanadia species, such as specific oxide support, and temperature, since the oxygen mobility on the catalyst surface is modified according to the increase in temperature and depends on the support.

To account for the competitive rate of SCR and ammonia oxidation as a function of temperature, a new NH_3/O_{active} concept was proposed taking into account the role of O_{active} in SCR mechanism, which was found to be similar to that of the OH radical in the SCR mechanism [61]. Based on the above explanations, it was concluded that the activity of SCR catalysts could be explained by the ratio between NH_3 adsorption sites and labile oxygen sources, which induces the dissociation of hydrogen-attached ammonia and/or the oxidation of NO to NO_2.

It is still not clear, however, in what proportion different active sites account for a redox behavior or for an acid–base interaction. For species such as vanadia, as well as molybdenum or tungsten oxides, the barrier between these states is very fragile. Actually, the Eley–Rideal model involves the adsorption of ammonia on V=O (V(V) sites) with a subsequent NO interaction with the dissociatively adsorbed (NH_x) species. Data obtained with these catalysts indicate that, under the reaction conditions, a better dispersion of vanadium in very high surface area catalyst allows the chemisorption of ammonia on the Lewis acid sites. DRIFT results indicated a predominance of the chemisorbed species on these sites.

A correlation of the structural properties with catalytic performance leads to the conclusion that, as demonstrated also in the present work, good reactivity is combined with the presence of surface isolated monovanadate species, $O{=}V{-}(O{-}M)_3$. Previous in situ Raman studies during SCR, considering ^{18}O labeling of the terminal oxygen, indicated that the lifetime of V=O is ~ 10 times the characteristic reaction time and that the V–O–M (M = support metal atom) is involved in the rate-determining step [52,60]. As a result, in the suggested NH_3/O_{active} ratio, O_{active} appears to be directly correlated with the $O{=}V{-}(O{-}M)_3$ concentration.

Accordingly, the higher acidity (Ti–O–Si, V–O–Si, V–O–Ti) and active redox site (V=O) observed on VTSN5 confirm that the SCR activity can be explained by the dual-site mechanism, as proposed by Topsøe et al. [54,55] (Scheme 1). In particular, the very high selectivity obtained with this catalyst might be related to the increase in V=O dispersion due to the preparation method. Several authors stressed the fact that N_2O desorbed after reaction is related to a Langmuir–Hinshelwood mechanism [62,63]. We suppose that such a reaction route is favored mainly on large vanadia aggregates. In the case of our catalysts, even for those that contain oligomerized species, the relatively high surface area allows good dispersion. Under such conditions the Eley–Rideal route is favored.

However, based on the mechanism proposed by Odriozola et al. [64], who suggested that TiO_2 is adsorbing NO, in the present case the close proximity of vanadia and titania may provide sources for chemisorption of both NH_3 and NO, thus increasing the catalytic activity.

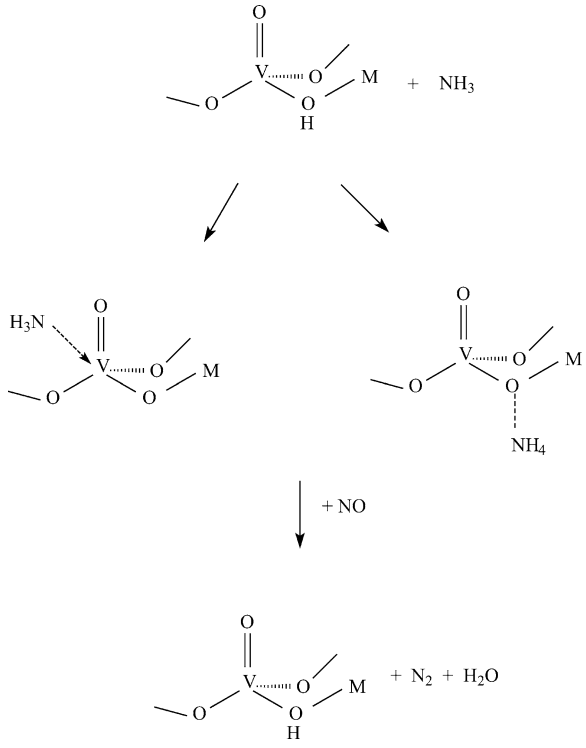

Scheme 1.

The behavior of VTSN1 and VTSN9 might be explained either by an advanced incorporation of vanadia that makes it inaccessible or by very unfavorable surroundings.

5. Conclusions

One-pot preparation of mixed V_2O_5–TiO_2–SiO_2 catalysts leads to high surface area materials in which both vanadia and titania exist in very high dispersion. Ordered textures such as MCM-41 may also result from these preparations. Vanadia is entrapped in these catalysts as V(V) species in which the population of V=O monomeric bonds strongly depends on the dispersion. Titanium also exists in a very oxidated state, and for high dispersions it adopts a tetrahedral coordination.

These structures lead to surfaces on which mainly Lewis acid sites exist under reaction conditions. These sites may orient the reaction route after an Eley–Rideal mechanism, thus providing very high activity and selectivity. Comparison with a conventional V_2O_5–TiO_2 catalyst led to the conclusion that the intrinsic activity is higher if we express the activity in terms of amount of vanadia. But in terms of productivity, namely, by expressing the activity per gram of catalyst, one-pot prepared V_2O_5–TiO_2–SiO_2 catalysts provide better conversions. From an application point of view this is a very important aspect. Contrary to the low-surface-area TiO_2 support, such preparation procedures allow an increase in the amount of vanadia that might be introduced inside.

Another important improvement resulting from the preparation of these catalysts concerns the selectivity, which was in all cases higher than that observed using the conventional V_2O_5–TiO_2 catalyst.

Acknowledgments

NATO's Scientific Affairs Division in the framework of the Science for Peace Programme (SfP 971984) has sponsored this research. We also thank the National Fund for Scientific Research (FNRS), Belgium.

References

[1] F. Janssen, F. Van den Kerkhof, H. Bosch, J.J. Ross, J. Phys. Chem. 91 (1987) 5931.
[2] F. Roozeboom, M.C. Mittelmeijer-Hardeger, J.A. Moulijn, J. Medema, V.H.J. de Beer, P.J. Gellings, J. Phys. Chem. 84 (1980) 2783.
[3] T. Shikada, K. Fujimoto, T. Kunugi, H. Tominaga, S. Kaneko, Y. Kubo, Ind. Eng. Chem. Prod. Res. Dev. 20 (1981) 91.
[4] J. Blanco, P. Avila, C. Barthelemy, A.G. Valdenebro, Appl. Catal. 63 (1990) 403.
[5] H. Matralis, S. Fiasse, R. Castillo, Ph. Bastians, M. Ruwet, P. Grange, B. Delmon, Catal. Today 17 (1993) 141.
[6] K. Tanabe, M. Misono, Y. Ono, H. Hattori, in: New Solid Acids and Bases, Kodansha/Elsevier, Tokyo, 1989, p. 199.
[7] S.M. Jung, P. Grange, Catal. Today 59 (2000) 305.
[8] X. Gao, I.E. Wachs, Catal. Today 51 (1999) 233; references therein.
[9] D.C.M. Dutoit, M. Schneider, A. Baiker, J. Catal. 153 (1995) 165.
[10] G. Deo, A.M. Turek, I.E. Wachs, D.R.C. Huybrechts, P.A. Jacobs, Zeolite 13 (1993) 365.
[11] S. Imamura, S. Ishida, H. Tarumoto, Y. Saito, T. Ito, J. Chem. Soc. Faraday Trans. 89 (1995) 757.
[12] P. Wauthoz, M. Ruwet, T. Machej, P. Grange, Appl. Catal. 69 (1991) 149.
[13] A. Fernandez, J. Leyrer, A.R. Gonzalez-Elipe, G. Munuera, H. Knözinger, J. Catal. 112 (1988) 489.
[14] R. Castillo, B. Koch, P. Ruiz, B. Delmon, J. Mater. Chem. 4 (1994) 903.
[15] N.E. Quaranta, J. Soria, V. Cortes Corberan, J.L.G. Fierro, J. Catal. 171 (1997) 1.
[16] C.U.I. Odenbrand, P.L.T. Gabrielsson, J.G.M. Brandin, R.M. Anderson, A.H. Lars, Appl. Catal. 78 (1991) 109.
[17] E.I. Ko, J.P. Chen, J.G. Weissman, J. Catal. 150 (1987) 511.
[18] R.B. Bjorklund, C.U.I. Odenbrand, J.G.M. Brandin, L.A.H. Andersson, B. Liedberg, J. Catal. 119 (1989) 187.
[19] R.A. Rajadhyaksha, H. Knözinger, Appl. Catal. 51 (1989) 81.
[20] A. Baiker, P. Dollenmeier, M. Glinski, A. Reller, Appl. Catal. 35 (1987) 365.
[21] M.G. Reichmann, A.T. Bell, Appl. Catal. 32 (1987) 315.
[22] T. Shikada, K. Fujimoto, T. Kunugi, H. Tominaga, J. Chem. Technol. Biotechnol. A 33 (1983) 446.
[23] C.U.I. Odenbrand, S.T. Lundin, L.A.H. Andersson, Appl. Catal. 18 (1985) 335.
[24] E.T.C. Vogt, A. Boot, A.J. Van Dillen, J.W. Geus, F.J.J. Janssen, F.M.G. Van den Kerkhof, J. Catal. 114 (1988) 313.
[25] R.A. Rajadhyaksha, G. Hausinger, H. Zeilinger, A. Ramstetter, H. Schmelz, H. Knözinger, Appl. Catal. 51 (1989) 67.
[26] B.E. Handy, A. Baiker, M.S. Marth, A. Wokaun, J. Catal. 133 (1992) 1.
[27] M.A. Reiche, E. Orteli, A. Baiker, Appl. Catal. B 23 (1999) 187.

[28] A. Sorrentino, S. Rega, D. Sannino, A. Magliano, P. Ciambelli, E. Santacesaria, Appl. Catal. A 209 (2001) 45.
[29] S.M. Jung, P. Grange, Appl. Catal. B 32 (2001) 123.
[30] I. Kawada, M. Nakano, M. Saeki, M. Ishii, N. Kimizuka, M. Nakahira, J. Less-Common Met. 32 (1973) 171.
[31] F.J. Berry, M.E. Brett, R.A. Marbrow, W.R.J. Patterson, Chem. Soc. Dalton Trans. (1984) 985.
[32] B. Horvath, J. Strutz, J. Geyer-Lippmann, E.G. Horvath, Z. Anorg. Allg. Chem. 483 (1981) 181.
[33] M.A. Stranick, M. Houalla, D.M. Hercules, J. Catal. 106 (1987) 362.
[34] A.Y. Stakheev, E.S. Shapiro, J. Apijok, J. Phys. Chem. 97 (1993) 5668.
[35] G. Went, L.-J. Leu, A.T. Bell, J. Catal. 134 (1992) 479.
[36] I.E. Wachs, Catal. Today 27 (1996) 437.
[37] I.E. Wachs, B.M. Weckhuysen, Appl. Catal. A 157 (1997) 67.
[38] I. Giakoumelou, Ch. Fountzoula, Ch. Kordulis, S. Boghosian, Catal. Today 73 (2002) 255.
[39] M. Amiridis, R.V. Duevel, I.E. Wachs, Appl. Catal. B 20 (1999) 111.
[40] M.A. Vuurman, D.J. Stufkens, A. Oskam, G. Deo, I.E. Wachs, J. Chem. Soc. Faraday Trans. 92 (1996) 3259.
[41] J.P. Dunn, P.R. Koppula, H.G. Stenger, I.E. Wachs, Appl. Catal. B 19 (1998) 103.
[42] G. Went, L.-J. Leu, S.J. Lombardo, A.T. Bell, J. Phys. Chem. 96 (1992) 2235.
[43] G. Went, S.T. Oyama, A.T. Bell, J. Phys. Chem. 94 (1990) 4240.
[44] J.P. Dunn, J.-M. Jehng, D.S. Kim, L.E. Briand, H.G. Stenger, I.E. Wachs, J. Phys. Chem. B 102 (1998) 6212.
[45] X. Gao, S.R. Bare, B.M. Weckhuysen, I.E. Wachs, J. Phys. Chem. B 102 (1998) 10842.
[46] S. Xie, E. Iglesia, A.T. Bell, Langmuir 16 (2000) 7164.
[47] P. Van Der Voort, M. Baltes, E.F. Vansant, J. Phys. Chem. B 103 (1999) 10102.
[48] X. Gao, S.R. Bare, J.L.G. Fierro, I.E. Wachs, J. Phys. Chem. B 103 (1999) 618.
[49] S.C. Su, A.T. Bell, J. Phys. Chem. B 102 (1998) 7000.
[50] J.P. Dunn, J.-M. Jehng, D.S. Kim, L.E. Briand, H.G. Stenger, I.E. Wachs, J. Phys. Chem. B 102 (1998) 6212.
[51] F.D. Hardcastle, I.E. Wachs, J. Phys. Chem. 95 (1991) 5031.
[52] M.A. Banares, I.E. Wachs, J. Raman Spectrosc. 33 (2002) 359.
[53] M.A. Centeno, I. Carrizosa, J.A. Odriozola, Appl. Catal. B 29 (2001) 307.
[54] N.-Y. Topsøe, Science 265 (1994) 1217.
[55] J.A. Dumesic, N.-Y. Topsøe, H. Topsøe, Y. Chen, T. Slabiak, J. Catal. 163 (1996) 409.
[56] G. Centi, S. Perathomer, J. Catal. 152 (1995) 93.
[57] G. Ramis, L. Yi, G. Busca, Catal. Today 28 (1996) 373.
[58] F. Kapteijn, L. Singoredjo, A. Andreini, J.A. Moulijn, Appl. Catal. B 3 (1994) 173.
[59] A.V. Salker, W. Weisweiler, Appl. Catal. 203 (2000) 221.
[60] I.E. Wachs, G. Deo, B.M. Weckhuysen, A. Andreini, M.A. Vuurman, M. de Boer, M.D. Amiridis, J. Catal. 161 (1996) 211.
[61] S.M. Jung, P. Grange, Appl. Catal. B 36 (2002) 207.
[62] M. Kantcheva, V. Bushev, D. Klissurski, J. Catal. 145 (1994) 96.
[63] J. Blanco, P. Avila, S. Suarez, J.A. Martin, C. Knapp, Appl. Catal. B 28 (2000) 235.
[64] J.A. Odriozola, H. Heinemann, G.A. Somorjai, J.F. Garcia de la Banda, P. Pereira, J. Catal. 119 (1989) 71.